Numerical and experimental investigation of impact of CO2 hydrates on rock permeability

Riano Castaneda, J.; Kahrobaei, S.; Aghajanloo, M.; Voskov, D.; Farajzadeh, R.

DOI
10.1016/j.fuel.2024.133708

Publication date
2024

Document Version
Final published version

Published in
Fuel

Fuel 381 (2025) 133708

Contents lists available at ScienceDirect

Fuel

journal homepage: www.elsevier.com/locate/fuel

Full Length Article

Numerical and experimental investigation of impact of CO_2 hydrates on rock permeability

J.Riano Castaneda [a], S. Kahrobaei [c], M. Aghajanloo [a], D. Voskov [a,b], R. Farajzadeh [a,c,*]

[a] Delft University of Technology, the Netherlands
[b] Department of Energy Resources Engineering, Stanford University, United States
[c] Shell Global Solutions International B.V., the Netherlands

ARTICLE INFO

Keywords:
Depleted gas fields
CO_2 hydrate
Joule-Thomson cooling
Injectivity

ABSTRACT

The reduction of temperature caused by Joule-Thomson effect during injection of CO_2 in low pressure reservoirs combined with presence of water can lead to formation of hydrates, which in turn reduces rock permeability and hence CO_2 injectivity. This paper introduces an empirical model to evaluate impact of hydrate formation on injectivity of CO_2 injection wells. Experiments were also conducted to validate the model. The model was then used to simulate injection of CO_2 into a multi-layered depleted gas field. The results indicate that operational parameters, particularly CO_2 injection rate and temperature, have a large influence on hydrate formation. This is because a higher CO_2 injection rate leads to a greater pressure drop within the injection well, potentially triggering conditions conducive to hydrate formation. It is also shown that the dynamics of the competition between the dry-out and temperature fronts play an important role in the final saturation of the hydrate within porous media. For large evaporation rates, the evaporation of water reduces water saturation near wellbore and hence formation of hydrates is limited.

1. Introduction

Among geological formations, depleted hydrocarbon reservoirs are especially attractive for storing CO_2 [8,12,9,19,6]. These formations have proven to be secure traps for storing CO_2 and have been largely characterized while extracting hydrocarbons. Therefore, there is a large amount of data available for any new development, including models to predict the movement of fluids in the reservoir. Moreover, production and injection history are useful to determine the CO_2 injection rate as well as the total amount of hydrocarbons produced helps to initially estimate the CO_2 storage capacity. Additionally, the existing infrastructure, including wells and facilities, may be suitable to be utilized by carbon capture and storage (CCS) projects.

Nevertheless, there are some potential challenges associated with storing CO_2 in depleted reservoirs [8,15,12,6,10]. Legacy well penetrations in depleted reservoirs can pose a potential risk of leakage. The utilization of existing infrastructure may be limited by the integrity of the materials not originally designed for CO_2 injection. In addition, the depletion status of the reservoirs can lead to Joule-Thomson (JT) cooling effect, as CO_2 expands from injection pressure to low reservoir pressure. Furthermore, despite the proven storage capacity in depleted reservoirs, potential containment risks in the near-wellbore region (due to low temperatures) need to be understood and managed.

One of the challenges encountered during storage of CO_2 in depleted gas reservoirs is the reduction in injectivity resulting from the formation of CO_2 hydrates within the reservoir due to the cooling effect caused by isenthalpic expansion of CO_2 [1,2]. Injectivity is defined as the ease with which the fluids can flow through a formation [14]. Injectivity is quantified through the injectivity index (J), which is the ratio of fluid rate injected (q_i) to the differential pressure (ΔP) required to maintain the injection rate:

$$J = \frac{q_i}{\Delta P} \tag{1}$$

It is known, from Darcy law that flowrate (q) is related to permeability (K), which refers to the ability of a rock to allow fluids to flow through it. Permeability is dependent on the flow paths through which fluid can flow; therefore, the presence of hydrates reducing or obstructing flow paths directly affects injectivity. To assess the impact of hydrates on permeability, saturation of hydrate should be known, which can be calculated based on the reaction explained later. Several permeability models have been proposed to predict the dynamic permeability evolution of sediments containing gas hydrates. These

* Corresponding author at: Delft University of Technology, the Netherlands.
E-mail address: r.farajzadeh@tudelft.nl (R. Farajzadeh).

https://doi.org/10.1016/j.fuel.2024.133708
Received 8 August 2024; Received in revised form 19 October 2024; Accepted 9 November 2024
Available online 15 November 2024

Nomenclature

BPR	Back Pressure Regulator
BHP	Burr hole Pressure
C	fitting parameter (Chen Model)
CCS	Carbon Capture and Storage
DP	Differential Pressure
HIs	Hydrate Inhibitors
JT	Joule-Thomson
k	Permeability
k_b	backward reaction rate coefficient
k_f	forward reaction rate coefficient
k_{rw}	relative permeabilities of the aqueous phase
k_{rg}	relative permeabilities of the gas phase
MFC	Mass Flow Controller
MSE	Mixed-Solvent-Electrolyte
NIST	National Institute of Standards and Technology
n_{Hyd}	hydration number
P	Pressure/Pressure Transducer
r	reaction rate
T	Temperature
TC	Thermocouple
t	time
S_w	Water saturation
S_{wc}	irreducible-water saturation
S_{gr}	residual-gas saturation
SRK	Soave-Redlich-Kwong
q	injection fluid rate
J	injectivity index

Subscript & Superscript

H	hydrate
inj	injection
b	backward
f	forward
w	water

Greek Character

ΔP	pressure difference
β	constant/formation damage coefficient (Pang-Sharma model)

models employ various methods, such as theoretical derivation or empirical fitting, and consider different assumptions, including the morphology and distribution of hydrates within the porous space [27]. The morphology of hydrates in porous media (pore filling, grain-coating, cementing, load-bearing, and patchy distribution) has a distinct impact on permeability and results in a different permeability model.

Effective storage of CO_2 in depleted gas fields therefore requires assessment of the potential impact of CO_2 hydrates on injectivity (decline). This study aims to investigate and evaluate the effect of CO_2 hydrates formation when injecting CO_2 in depleted gas reservoirs, employing a combination of experimental and modeling approaches. In general modeling of hydrates in porous media is very challenging and to date there is no simulator that can fully simulate the impact of hydrates (as a result of cold CO_2 injection) on reservoir permeability. Commercial reservoir simulators suffer from numerical stability when conversion of phases is considered. In the case of hydrate formation, a solid CO_2 phase appears in addition to gaseous and liquid CO_2, which adds further to the complexity of the non-*iso*-thermal simulations process, especially at reservoir scale. Therefore, there is a need for development of simpler models which can be used to assess the risk of hydrate formation during CCS in depleted fields. The focus of this paper is to develop a fit-for-purpose and empirical model with parameters obtained from well-designed experiments. The model is designed to simulate the formation and dissociation of hydrate in porous media, and eventually to estimate its impact on reservoir properties such as porosity and permeability. The empirical model aims to support hydrate risk assessment during CO_2 injection into depleted gas reservoirs, aiding in the planning and design of CCS projects. Experimental results will also be essential for calibration of the modeling approach. The results of the developed model provide insights into propagation of the cold temperature front and hydrate formation on flow dynamics, based on which mitigation or prevention strategies can be designed.

The structure of the paper is as follows. Section 2 focuses on the experimental setup and procedure. Section 3 is dedicated to the modeling approach, description of key aspects of the models including simulation of the experiments. A comprehensive discussion of the obtained results and their implications are provided in Sections 4 to 6. Section 7 presents the concluding remarks and recommendations for future research.

2. Experiments

To study the impact of CO_2 hydrates on the injectivity of CO_2 into porous media, several laboratory experiments were conducted using a specifically designed setup. The tests were based on a core-flooding experiment, where CO_2 was injected into a core sample with well-defined properties such as porosity, permeability, and initial water saturation.

2.1. Experimental setup

An experimental setup was designed to perform a core flooding experiment maintaining thermodynamic conditions (P and T) within the hydrate stability zone to provide sufficient driving force for hydrate formation. The setup comprises three sections: the inlet section, the central section, and the outlet section, as schematically shown in. The inlet section involves injecting fluids into the core using a Vindum Pump for solutions and mass flow controller for gases. To ensure fluids enter the core at the desired experimental temperature, spiral lines are employed inside the cooler along the injection lines to extend the flow path. The central section consists of the core which is placed inside a core holder located within a cooler to control the temperature for hydrate formation and dissociation. The measurement equipment includes two thermocouples, four pressure transducers, and two differential pressure sensors. The schematic in Fig. 1 illustrates the placement of these sensors. The outlet section includes a valve that connects to both the vacuum pump and the back pressure. The back pressure is utilized to maintain the system at a specific pressure throughout the entire experimental process. The Bentheimer sandstone (91.6 % quartz, 2.5 % kaolinite, 5.0 % K-feldspar, 0.9 % other) investigated in this study is characterized by a porosity of 23 % and a permeability of 1.8 D [17]. The core measures 17 cm in length and 3.8 cm in diameter. The salinity of the brine used in all experiments was 1 wt% NaCl.

2.2. Experimental procedure

Initially, the core is saturated with brine to the desired level by co-injecting N_2 and brine solution at a fixed fraction. The details of the saturation process can be found in [1,2]. The core is then pressurized up to 30 bar and the fridge temperature is set to 1 °C resulting in an internal core temperature of 1.5 ± 0.5 °C. A permeability test is conducted by

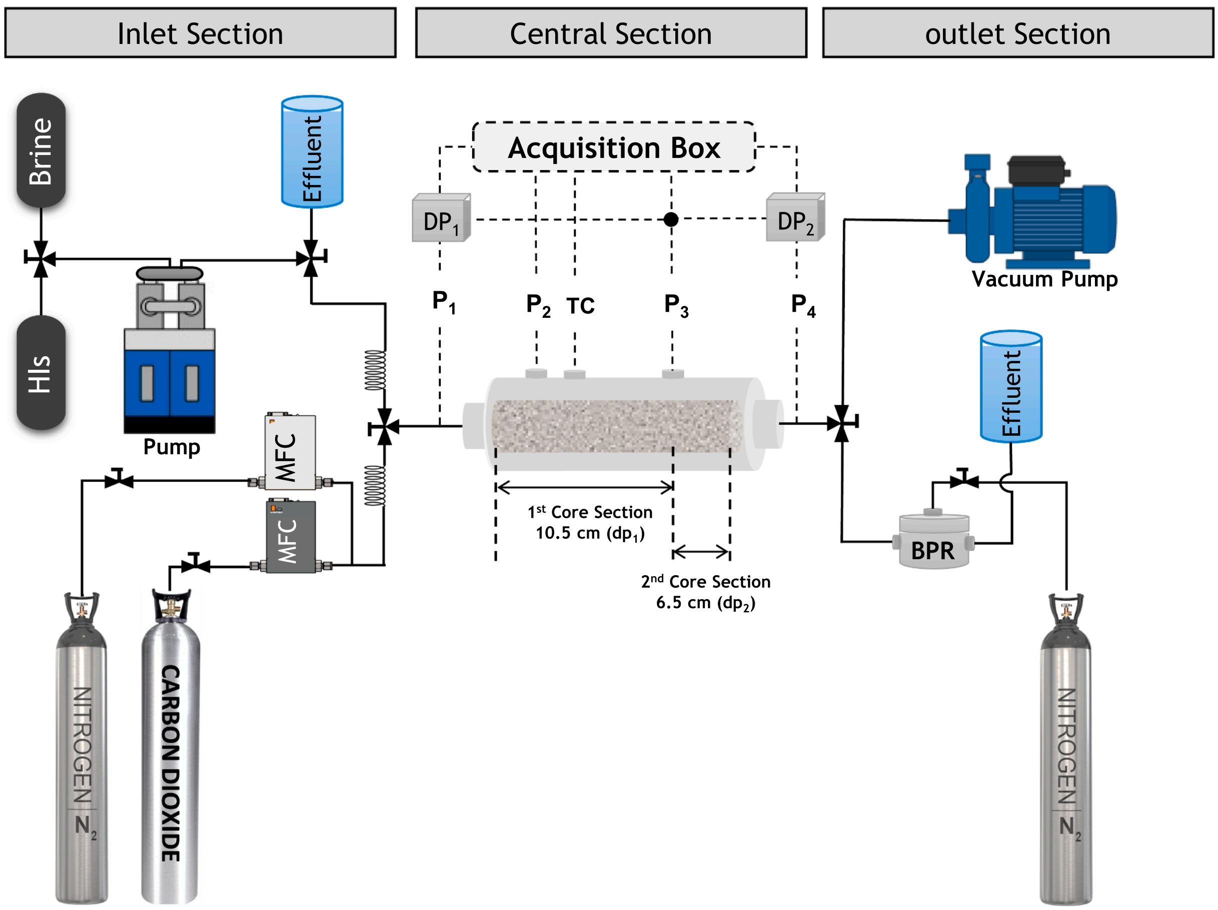

Fig. 1. Schematic of the experimental setup for dynamic gas hydrate experiments. Back Pressure Regulator (BPR), Differential Pressure(DP); Hydrate Inhibitors (HIs); (MFC) Mass Flow Controller; (P) Pressure Transducer; (TC) Thermocouple.

varying the injection rate and measuring the core differential pressure for each selected rate followed by injection of at least 5 PV (pore volume) of brine to establish the baseline. Afterwards, the injection of CO_2 started at a constant rate of 5 g/h. A pressure drop from the baseline and an increase in temperature are indicators of macroscopic hydrate nucleation time. CO_2 injection continued until the end of the growth phase, where the pressure stabilized.

3. Numerical model

3.1. General features

A comprehensive thermal model is developed to simulate a five-phase system, which includes water, liquid, gas, and two solid phases, specifically hydrate and salt. Shell's in-house Modular Reservoir Simulator (MoReS) [18,20] is utilized for flow simulations. The components include H_2O, CO_2, CH_4, CO_2 hydrate, and salt, to represent the main components initially present in a gas reservoir, see Fig. 2. H_2O primarily exists in the water phase but can partition into the CO_2 phase. CO_2 can coexist in both liquid and gaseous states and can partition into the water phase. Salt can coexist in both water and salt phases, while hydrate consistently remains in the hydrate phase. Depending on the pressure and temperature, CO_2 may undergo phase transitions during the simulation. The properties of CO_2 are derived from the Span and Wagner Equation of State [23]. Water properties are obtained from National Institute of Standards and Technology (NIST) database [11]. CH_4 properties are derived from the Setzmann and Wagner model [21]. All properties have undergone rigorous benchmarking against the NIST. Furthermore, the model can simulate H_2O-CO_2 partitioning. The

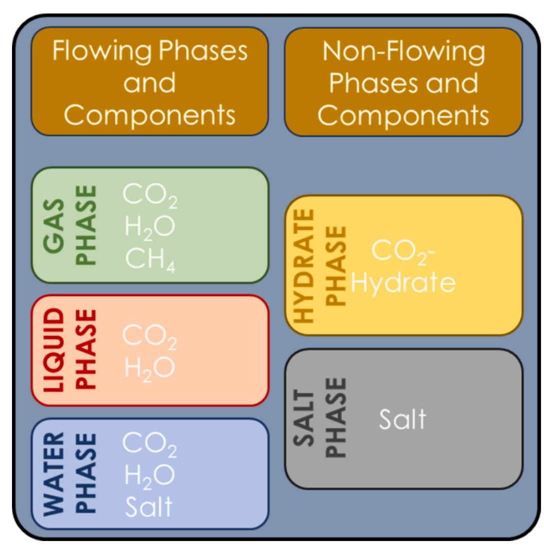

Fig. 2. Flowing and non-flowing phases and their components in the model.

Spycher model [25] is employed to model H_2O evaporation and CO_2 solubility in water at zero salinity. The MSE-SRK model in OLI-Studio [24] is employed to define H_2O-CO_2 partitioning at non-zero salinities. This model is based on the Mixed-Solvent-Electrolyte (MSE) model [26] for electrolyte systems but utilizes the modified Soave-Redlich-Kwong (SRK) equation of state [22] for both the gas phase and the second liquid (or nonelectrolyte) liquid phase. The density of a CO_2 hydrate is assumed to be constant [7]. The molecular weight of the CO_2 hydrate is calculated 182.6 g/mol considering a hydration number of 7.7. The model operates in a thermal mode, accounting for temperature-dependent fluid compositions, porosity, enthalpy, density, and viscosity. It also considers heat conductivity and rock heat capacity, which can be included if specified. Additionally, the model can incorporate heat loss to the overburden and underburden when specified.

3.2. Hydrate formation and dissociation

To simulate hydrate formation and dissociation, an empirical approach is adapted that determines whether the conditions are conducive for hydrate formation at a specific pressure and temperature. The model defines the gas hydrate equilibrium curve based on the concentration of salt, in this case NaCl. These equilibrium curves are derived through regression analysis of the hydrate pressure–temperature (PT) diagram, resulting in a set of fitting parameters as a function of NaCl concentration. The comparison between the fitting curves and the hydrate PT diagram obtained from a thermodynamic package Hydraflash is shown in Fig. 3.

In our model, the process of hydrate formation and dissociation are governed by the thermodynamic conditions outlined in the hydrate phase diagrams, as shown in Fig. 3. The model evaluates the pressure and temperature of each grid-block at each time step against the defined phase diagram. If these conditions fall within the hydrate stability zone and both water and CO_2 co-exist, hydrate formation is triggered. Conversely, for grid blocks with hydrate saturation of larger than zero, if the pressure and temperature conditions shift outside the hydrate stability zone, hydrate dissociation ensues. This process is visually demonstrated in Fig. 4 for a specific salinity level.

Since Salt cannot be incorporated into the hydrate structure and given the higher solubility of CO_2 compared to CH_4, as well as the fact that the thermodynamic conditions (20–30 bar) are more favorable for CO_2 hydrate formation compared to CH_4, the reactions describing formation and dissociation of CO_2 hydrate are represented by the following equation [4]:

$$n_{Hyd}H_2O + CO_2 \Leftrightarrow^{k_f} k_b\, Hydrate \quad (2)$$

where, n_{Hyd} is the hydration number (7.7 in this study, based on the assumption of semi-filling of hydrate cages), k_f and k_b are, respectively, the forward and backward reaction rate coefficients. These coefficients are calculated by

$$r_f = k_f[H_2O]^{n_{Hyd}}[CO_2] \quad (3)$$

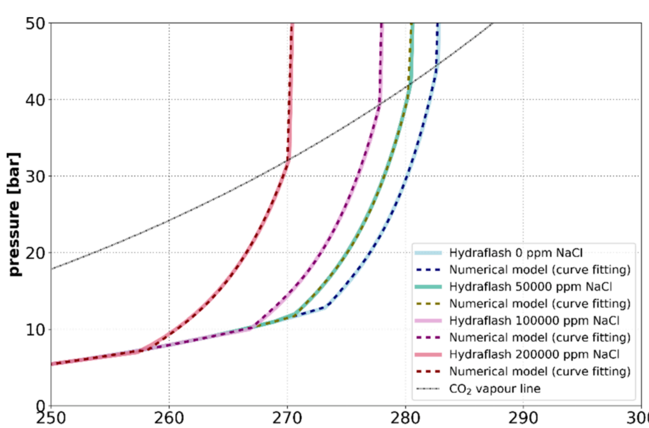

Fig. 3. PT phase diagrams showing the hydrate equilibrium curve depending on the salinity in the system. The solid lines in the diagrams represent the results obtained from HydraFlash, while the dashed lines depict the outcomes of the curve fitting process.

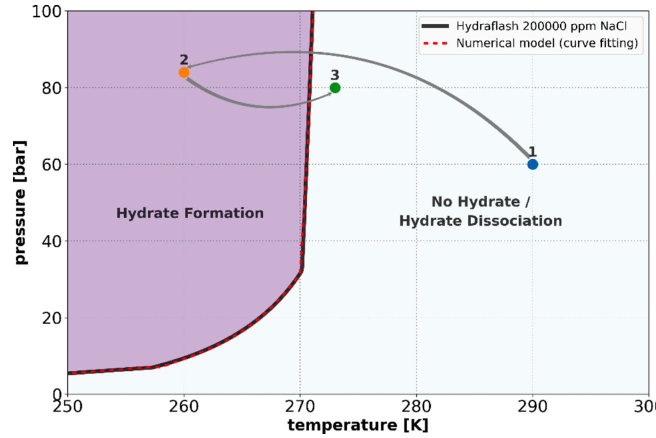

Fig. 4. Formation and dissociation of hydrate: Hydrate forms when water and CO2 saturations are above zero and pressure and temperature fall inside the purple area. Hydrate dissociates when conditions of the grid block move outside of the purple zone. (For interpretation of the references to color in this figure legend, the reader is referred to the web version of this article.)

$$r_b = k_b[Hydrate] \quad (4)$$

where, the square brackets ([]) denote the concentration of components and r_f and r_b denote the forward and backward reaction rate, respectively.

To model impact of hydrate on permeability (k/k_0), two well-known models were used. The first model is a function of hydrate saturation (S_H) and a constant (β) so called formation damage coefficient that accounts for trapped solids in the pores [16]:

$$\frac{K}{K_0} = \frac{1}{1+\beta S_H} \quad (5)$$

The second model (Chen model) proposes a modified Corey model with an exponential function of hydrate saturation (S_H), which includes a fitting parameter (C) that indicates the degree of crystal coarsening and patch size for a multiphase system [27]:

$$\frac{K}{K_0} = (1 - S_H)\exp(-CS_H) \quad (6)$$

Fig. 5 compares data of [1,2] with these two models.

4. Model Validation

The model was validated by simulating the pressure data measured

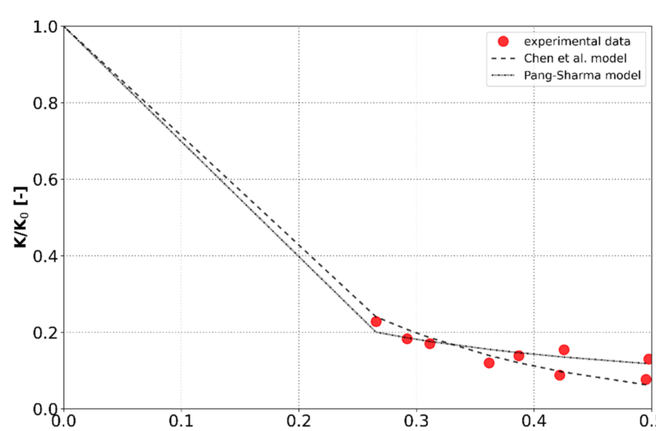

Fig. 5. Permeability prediction as a function of hydrate saturation based on Pang-Sharma and Chen et al. models.

from the coreflood experiments. A total of 9 experiments were conducted using a 1 wt% NaCl solution under initial conditions of 30 bar and 1 °C. The measured pressure data along the core length serves as an indicator of permeability reduction due to hydrate formation. It is important to note that the experimental conditions allowed for the disregard of H_2O-CO_2 partitioning due to the low temperature of the experiments ($T = 1$ °C). The empirical model was developed based on the Chen et al. model and the Peng and Sharma model to quantify the permeability damage because of hydrate formation. The rate of hydrate formation (k_f in Eq. (3), the β parameter (for the Pang and Sharma approach; see Eq. (5), and the exponent C (for the Chen et al. approach; see Eq. (6) were employed as tuning parameters. The experimental conditions for these experiments never entered the hydrate dissociation region and consequently the dissociation rate did not influence the simulations.

To replicate the core-flooding experiment, a 1D Cartesian grid with logarithmic gridding was constructed, mirroring the core dimensions and properties, primarily permeability and porosity. An injector, constrained by a volume rate, was positioned at the left edge of the model, while a producer, constrained by a bottom-hole pressure equivalent to the initial core pressure, was placed at the right edge of the system. The injection temperature is set at a constant 1 °C, replicating the experimental conditions. The model properties and simulation parameters used in the simulation of the experiments are outlined in Table 1. The values for the CO_2-water relative permeability curves, derived from a core flooding experiment conducted on a Bentheimer core as detailed in Eftekhari and Farajzadeh [5], are presented in Table 2. The initial conditions of each experiment utilized for history matching are depicted in Table 3.

Figs. 6–8 display the results of the simulated pressure for the three distinct experiments. The pressure exhibits a gradual increase over time, attributable to the formation of hydrates. The rate of this pressure increase in the model is adjusted by altering the value of k_f, which represent the rate of hydrate growth in porous media. A larger value results in a steeper slope of the pressure curve. Note that the hydrate nucleation and growth rate strongly depends on small scale heterogeneity in the core. Due to the presence of excess CO_2 and low salinity of the brine, it is assumed that nearly all water molecules are consumed in

Table 1
Model properties and simulation parameters for simulation of the experimental data.

Category	Property	Value	Unit
Grid	Number of cells in X-direction	200	[-]
	Number of cells in Y-direction	1	[-]
	Number of cells in Z-direction	1	[-]
	Length (X)	17.00	[cm]
	Width (Y)	3.37	[cm]
	Height (Z)	3.37	[cm]
Rock	Porosity	0.23	[-]
	Permeability	2,200	[mD]
	Rock heat capacity	1,000	[J/kg/K]
	Rock density	2,600	[kg/m3]
	Formation thermal conductivity	0	[W/m/K]
Model	Heat exchange with surrounding rock	No	
	Capillary pressure	No	
	CO_2-H_2O partitioning	No	
	Relative permeability curves	CO_2-water curves	
Wells	Wellbore radius	0.0001	[cm]
	T_{inj}	1	[°C]
	CO_2 injection rate	1	[ml/min]
	Injection constraint	Constant injection rate, maximum BHP	
	Production constraint	Minimum BHP	

Table 2
Corey parameters for the relative permeability model of a CO_2-water system, from [5].

Water			Gas (CO_2)		
S_{wc} [-]	k_{rw} [-]	n_w [-]	S_{gr} [-]	k_{rg} [-]	n_g [-]
0.05	0.720	4.423	0.03	0.587	0.938

Table 3
Initial conditions of the experiments.

	P [bar]	T [C]	S_{wi}
Exp #1	30.3	1.0	0.26
Exp #2	29.5	1.0	0.35
Exp #3	29.5	1.0	0.30

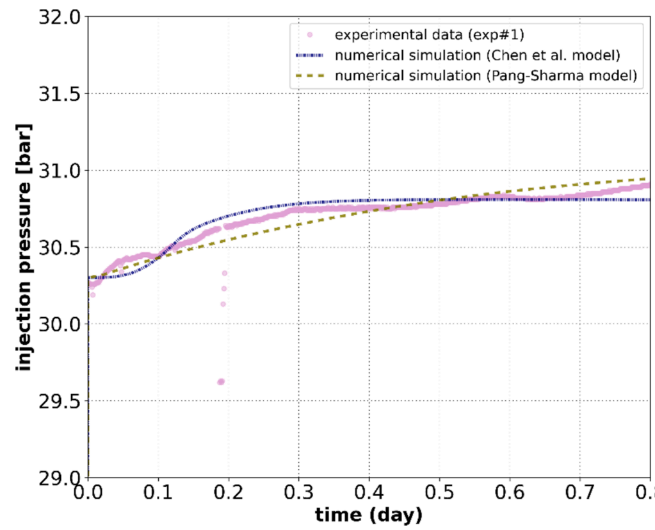

Fig. 6. Simulated pressure versus measured data for experiment # 1 using Chen et al. and Pang-Sharma models.

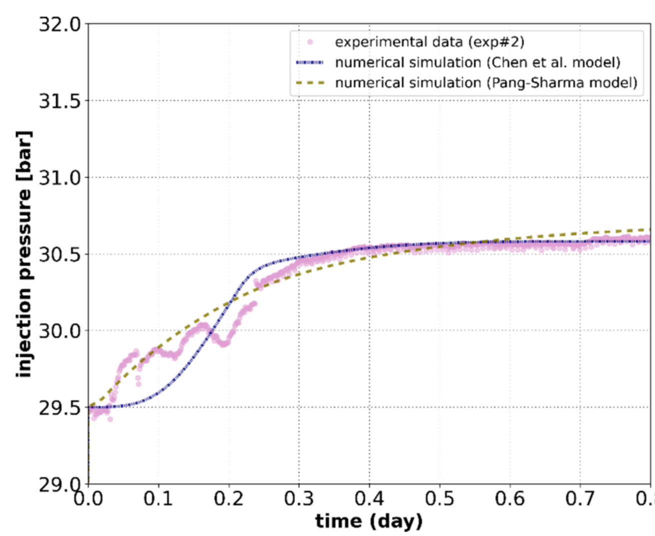

Fig. 7. Simulated pressure versus measured data for experiment # 2 using Chen et al. and Pang-Sharma models.

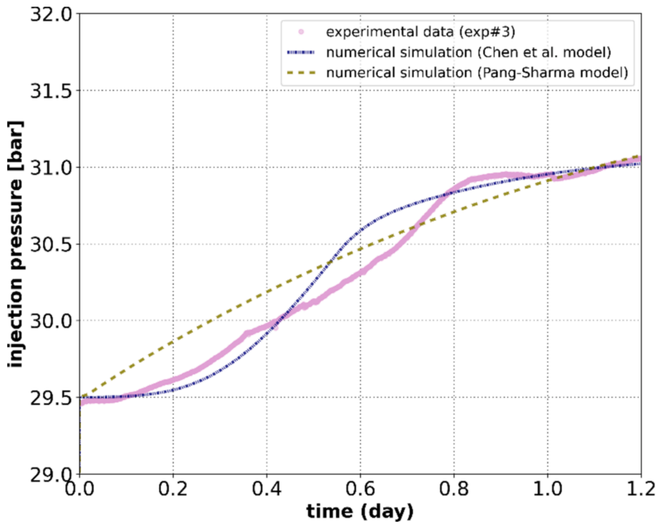

Fig. 8. Simulated pressure versus measured data for experiment # 3 using Chen et al. and Pang-Sharma models.

forming the hydrate structure, after which the pressure stabilizes. The magnitude of the pressure increase is matched by modifying the values of the β and C parameters in the Pang-Sharma and Chen et al. models, respectively. These parameters are summarized in Table 4.

5. Impact of hydrate formation on injectivity in a Multi-Layered reservoir

In this case study the model was used to investigate the impact of hydrate formation on injectivity in a multi-layered reservoir composed of 20 layers, however, the model is independent of the number of layers represented in the model. To illustrate the impact of hydrate formation on injectivity at a larger scale, two simulation cases were executed at two different injection temperatures: one at −5 °C (representative of conditions conducive to hydrate formation, inside the hydrate stability zone) and the other at 12 °C (represents conditions within hydrate safe zone, outside of the hydrate stability zone). A single-well radial model was constructed with a length of 1000 m and a height of 111 m. The model was assumed to have no-flow boundary conditions, effectively creating a closed system. The injection was constrained by a CO_2 mass rate of 1 Mt/year (~31 kg/s), and the injection temperature was assumed to remain constant at the sand face. Heat exchange with the over- and under-burden rocks and CO_2-H_2O partitioning were excluded in these simulations. The reservoir was initialized with CH_4 and 200,000 ppm saline brine at a connate water saturation of 0.2.

The Chen et al. model was employed to model the permeability damage due to formation of hydrate. The tuned parameters from experiment 3 were used for the hydrate formation rate and the C parameter. The hydrate dissociation rate was assumed to be equal to the formation rate. Drawing from experiences with various trials for polymer flooding [13] and foam injection [3], it was observed that the parameters achieved in the lab are typically at least one or two orders of magnitude larger than those achieved at the field scale. Therefore, using similar reasoning, the C parameter was also reduced by an order of magnitude as a reasonable approach for upscaling the parameter. The appropriate upscaling method should be defined when more field data is available for cold CO_2 injection. The main simulation parameters for this case are provided in Table 5. For replicability of the model, in case conditions such as lithology and salinity change, hydrate formation rate and the C parameter need to be calculated.

Fig. 9 displays the grid block pressure and temperature conditions behind the temperature front on the hydrate PT diagram with 200,000 ppm NaCl for two injection temperature scenarios: a) −5 °C and b) 12 °C. For the 12 °C injection scenario, the conditions in the grid blocks do not intersect with the hydrate stability zone, resulting in no hydrate formation. Conversely, for the −5°C scenario, the pressure and temperature in the grid blocks behind the cold temperature front fall within the hydrate stability zone, leading to hydrate formation. The red dots on these plots represent the grid block pressure and temperature values, while the black curve illustrates the hydrate PT diagram with 200,000 ppm NaCl salinity. The dotted-dashed blue line represents the injection temperature.

Fig. 10 depicts the temperature (top) and hydrate saturation (bottom) profiles in the reservoir after two years of injection for a) −5 °C and b) 12 °C cases, respectively. In the −5 °C injection case, hydrate formation extends up to 50 m from the injection well after two years, while no hydrate formation is observed in the 12 °C case. Note that the distance is plotted on a logarithmic scale.

To further illustrate the impact of hydrate formation on injectivity, the injection bottom-hole pressure is plotted as a function of time for both cases in Fig. 11. The hydrate formation in the −5 °C injection case results in approximately 40 % increase in the injection pressure compared to the 12 °C case with no hydrate formation. However, given the parameters used in the simulations particularly the low initial water

Table 4
Parameters used to history match the experiments.

Case	Model	β or C			k_f		
		Exp #1	Exp #2	Exp #3	Exp #1	Exp #2	Exp #3
1	Chen et al.	C = 22.5	C = 18	C = 22.31	1.8	1.58	0.48
2	Pang and Sharma	β = 7000	β = 7333.5	β = 18000	0.12	0.33	0.058

Table 5
Initial conditions and simulation parameters.

Category	Property	Value	Unit
Grid	Radius	1000	[m]
	Thickness	111	[m]
	Number of cells in-radial direction	100	[-]
	Number of cells in Z-direction	20	[-]
Initial Conditions	T	140	[°C]
	P	20	[bar]
	$S_{w,i}$	0.20	[-]
	Initial fluids in reservoir	CH_4 and Water	
	Salinity	200000 NaCl	[ppm]
Rock	Porosity	Variable per layer	[-]
	Permeability	Variable per layer	[mD]
	Rock heat capacity	1,000	[J/kg/K]
	Rock density	2,600	[kg/m3]
	Formation thermal conductivity	0	[W/m/K]
Model	Heat exchange with surrounding rock	No	
	Capillary pressure	No	
	CO_2-H_2O partitioning	No	
	Permeability reduction model	Chen et al.	
	Relative permeability curves	CO_2-water curves	
Hydrate	Formation/dissociation rates	0.48	[-]
	Chen et al. model exponent (C)	2.231	[-]
Wells	Wellbore radius	0.1	[m]
	T_{inj}	−5 or 12	[°C]
	CO_2 mass injection rate	1	[Mt/year]
	Injection constraint	Constant mass injection rate	

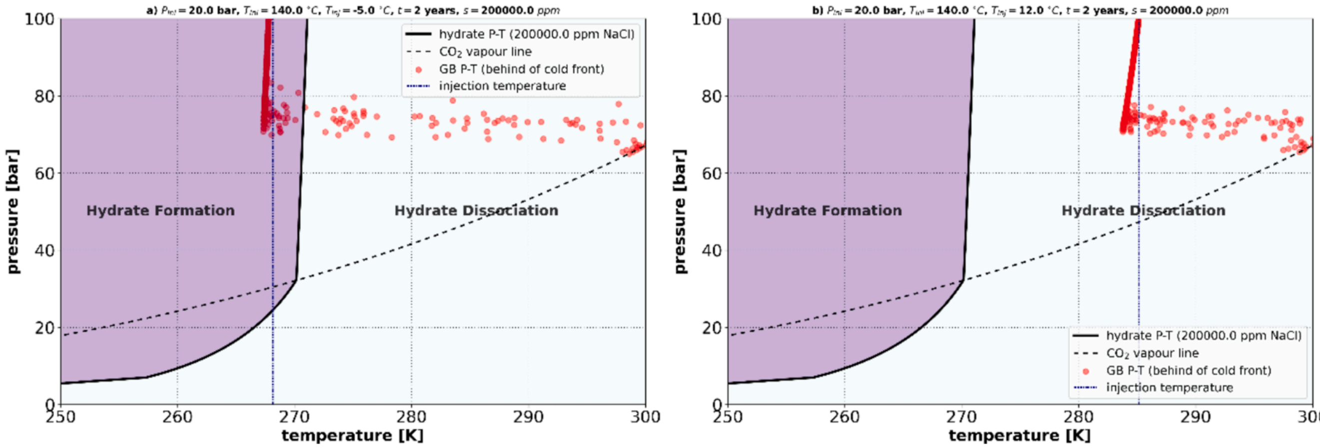

Fig. 9. Pressure and temperatures of the gridblocks behind the cold temperature front for the two simulated cases.

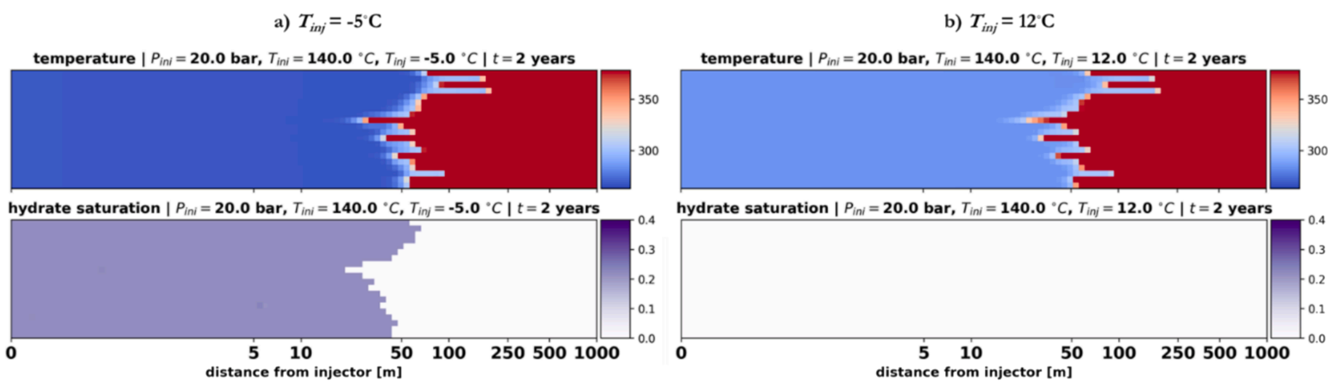

Fig. 10. Temperature (top) and hydrate saturation (bottom) profiles inside the reservoir for the two simulated cases.

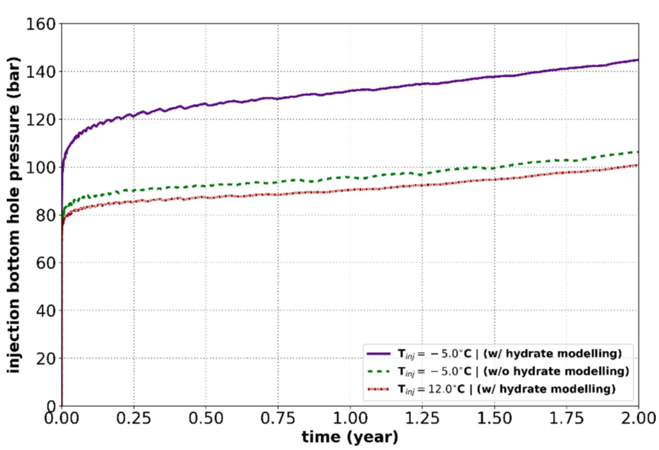

Fig. 11. Bottom-hole injection pressure as a function of time for three cases: −5 °C with hydrate formation (solid purple line), 12 °C with no hydrate formation (dotted-dashed red line), and −5°C without allowing hydrate to form (dashed green line). (For interpretation of the references to color in this figure legend, the reader is referred to the web version of this article.)

saturation, the hydrate formation has not led to a complete blockage or total loss of injectivity. Additionally, an extra case with an injection temperature of −5 °C, but without allowing hydrate formation, is included as a reference (dashed green line). This reference case demonstrates that the decrease in injectivity for the −5 °C case with hydrate formation, compared to the 12 °C case, is primarily due to hydrate formation. The difference between dashed-green and the red lines is because of the difference in CO_2 properties at different injection temperatures.

6. Impact of dry-out on hydrate formation

The formation of hydrates in the reservoir can be influenced by the competition between the dry-out and the rate of hydrate formation. In certain scenarios, such as those involving high reservoir temperatures, the dry-out front can outpace the cold front, leading to water evaporation ahead of the cold zone. Consequently, the amount of water available for hydrate formation can be reduced or, in some instances, eliminated. To investigate this, the model introduced in the previous section was used to study the effect of dry-out on hydrate formation by incorporating CO_2-H_2O partitioning into the simulations. However, it is important to note that in our simulations, CO_2-H_2O partitioning, or H_2O evaporation, is modeled at equilibrium, implying that it occurs instantaneously. This means the transient state of evaporation/dissolution is not considered. Dry-out can occur more slowly, resulting in less evaporation and the dry-out front spreads over larger distance.

Fig. 12**a** and Fig. 12**b** illustrate the temperature (top), water saturation (middle), and hydrate saturation (bottom) profiles after 2 years of injection for cases without dry-out included and with dry-out included, respectively, for an injection temperature of −5 °C. As can be seen from these profiles, the water saturation ahead of the hydrate saturation zone (corresponding to the cold zone) in the case that includes H_2O-CO_2 partitioning is reduced due to dry-out. This suggests that there is less water available for hydrate formation in this scenario. As a result, the hydrate saturation is lower compared to the case where dry-out is not considered.

Fig. 13 presents the bottom hole injection pressure for three distinct

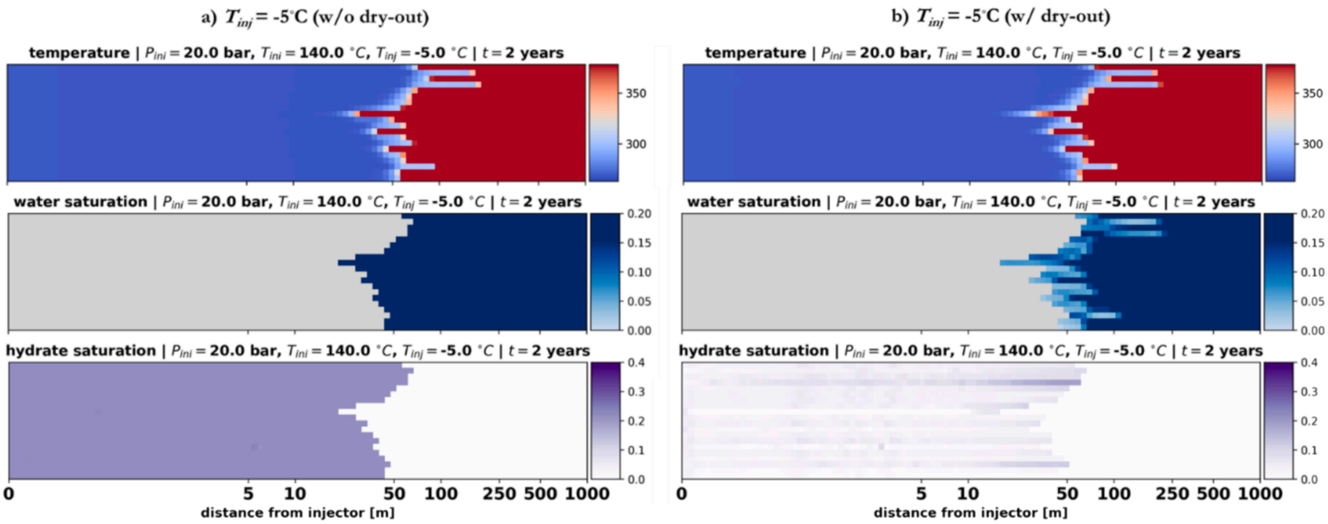

Fig. 12. Temperature (top), water saturation (middle) and hydrate saturation (bottom) profiles inside the reservoir for the two scenarios: a) without dry-out and b) with dry-out.

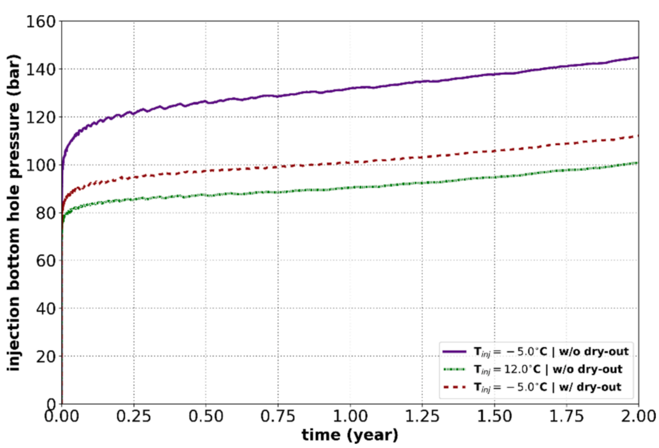

Fig. 13. Injection bottom hole pressure for the three scenarios: −5°C without dry-out (solid purple line),12°C without dry-out (dotted-dashed green line) and −5°C with dry-out (dashed red line). (For interpretation of the references to color in this figure legend, the reader is referred to the web version of this article.)

cases. The dark blue color represents an injection temperature of −5 °C without including CO_2-H_2O partitioning, indicating no dry-out. The dotted dashed green represents an injection temperature of 12 °C with no dry-out. The dashed dark red color represents an injection temperature of −5 °C, but with dry-out included. This figure demonstrates that for the case where dry-out is included, the injection pressure is approximately 20 % less compared to the case with the same injection temperature but without dry-out. This lesser reduction in injectivity is due to lower hydrate saturation, which is a result of less available water in the case where dry-out is included. However, it is important to note that the injectivity reduction due to salt precipitation is not considered in these simulations, which can further reduce the effective permeability.

7. Conclusions

This paper discussed a framework to evaluate impact of hydrate formation on injectivity of CO_2 injection wells. An empirical model was formulated to simulate hydrate formation and dissociation processes. Experiments were conducted, in which formation of hydrates resulted in reduction of effective permeability of the rock. The experimental data was used to obtain the model parameters, which included the kinetics of the reactions and hydrate saturation.

Both experimental and numerical approaches showed that the formation of hydrates leads to a reduction in permeability, thereby diminishing injectivity and elevating injection pressure. The operational parameters, particularly CO_2 injection rate and temperature, exert a large influence the risk of hydrate formation. The extent of the injectivity decline depends on the CO_2 temperature at the inlet boundary. For inlet temperatures within the hydrate stability zone, when there is sufficient water in the reservoir, hydrates form immediately in the vicinity of the well. However, for the case when the inlet temperature is outside of the hydrate stability zone, hydrate can still form away from the well due to expected low temperatures caused by the Joule-Thomson effect inside the reservoir, mainly in the vicinity of the injection well. Finally, the dynamics of the competition between the dry-out and temperature fronts play an important role in the final saturation of the hydrate within porous media. For large evaporation rates, the cold temperature front lags behind, resulting in reduced risk of hydrate formation. The impact of capillary-driven water backflow and water cross flow between layers needs further investigation.

CRediT authorship contribution statement

J.Riano Castaneda: Writing – original draft, Visualization, Formal analysis, Data curation. **S. Kahrobaei:** Writing – original draft, Software, Formal analysis. **M. Aghajanloo:** Writing – review & editing, Validation. **D. Voskov:** Supervision, Investigation. **R. Farajzadeh:** Writing – review & editing, Writing – original draft, Supervision, Formal analysis, Conceptualization.

Declaration of competing interest

The authors declare that they have no known competing financial interests or personal relationships that could have appeared to influence the work reported in this paper.

Acknowledgement

Authors thank Dr. Jeroen Snippe, Dr. Ali Fadili, and Dr. Marcella Dean for their valuable comments on the initial draft of this manuscript. Authors also acknowledge Shell Global Solutions International B.V. for permission to publish this work.

Data availability

Data will be made available on request.

References

[1] Aghajanloo M, Taghinejad SM, Voskov D, Farajzadeh R. Influence of water saturation and water memory on CO_2 hydrate formation/dissociation in porous media under flowing condition. Chem Eng J 2024;492:152455. https://doi.org/10.1016/j.cej.2024.152455.

[2] Aghajanloo M, Yan L, Berg S, Voskov D, Farajzadeh R. Impact of CO_2 hydrates on injectivity during CO_2 storage in depleted gas fields: A literature review. Gas Sci Eng 2024;123:205250. https://doi.org/10.1016/j.jgsce.2024.205250.

[3] Al-Abri M, Al Mahruqi D, Al-Aamri N, Das A, Kahrobaei S, van Batenburg D, et al. Derisking low-tension-gas flooding in a carbonate field in North Oman: results and insights from a successful foam-assisted WAG injection pilot. SPE Conf Oman Petrol & Energy Show 2024.

[4] Anderson GK. Enthalpy of dissociation and hydration number of methane hydrate from the Clapeyron equation. J Chem Thermodyn 2004;36(12):1119–27. https://doi.org/10.1016/j.jct.2004.07.005.

[5] Eftekhari AA, Farajzadeh R. Effect of foam on liquid phase mobility in porous media. Sci Rep 2017;7(1):43870. https://doi.org/10.1038/srep43870.

[6] English JM, English KL. An overview of carbon capture and storage and its potential role in the energy transition. First Break 2022;40:35–40. https://doi.org/10.3997/1365-2397.fb2022028.

[7] Ferdows M, Ota M. Density of CO_2 hydrate by monte carlo simulation. Proc Inst Mech Eng C J Mech Eng Sci 2006;220(5):691–6. https://doi.org/10.1243/09544062c13104.

[8] IPCC. (2005). Working Group III of the Intergovernmental Panel on Climate Change, Carbon Dioxide Capture and Storage. https://doi.org/https://digital.library.unt.edu/ark:/67531/metadc12051.

[9] Jenkins CR, Cook PJ, Ennis-King J, Undershultz J, Boreham C, Dance T, et al. Safe storage and effective monitoring of CO_2 in depleted gas fields. Proc Natl Acad Sci 2012;109(2):E35–41. https://doi.org/10.1073/pnas.1107255108.

[10] Kirchin, A. (2023). The comparative benefits of storage in depleted and deep saline reservoirs for CCS. RPS. https://doi.org/https://www.rpsgroup.com/insights/carbon-capture-and-storage/the-comparative-benefits-of-storage-in-depleted-and-deep-saline-reservoirs-for-ccs/.

[11] Linstrom P. National Institute of Standards and Technology. NIST Chemistry WebBook - SRD 2024;69. https://doi.org/10.18434/T4D303.

[12] Loizzo M, Lecampion B, Bérard T, Harichandran A, Jammes L. Reusing O&G-depleted reservoirs for CO_2 storage: pros and cons. SPE Projects, Facil & Constr 2010;5(03):166–72. https://doi.org/10.2118/124317-pa.

[13] Lotfollahi M, Farajzadeh R, Delshad M, Al-Abri A-K, Wassing BM, Al-Mjeni R, et al. Mechanistic simulation of polymer injectivity in field tests. SPE J 2016;21(04):1178–91. https://doi.org/10.2118/174665-pa.

[14] Manjunath GL. Chapter 9 - Formation damage in oil reservoirs during CO_2 injection. In: Sharma T, Chaturvedi KR, Trivedi JJ, editors. Nanotechnology for CO_2 Utilization in Oilfield Applications. Gulf Professional Publishing; 2022. p. 147–66. https://doi.org/10.1016/B978-0-323-90540-4.00001-6.

[15] Oldenburg CM. Joule-Thomson cooling due to CO_2 injection into natural gas reservoirs. Energ Conver Manage 2007;48(6):1808–15. https://doi.org/10.1016/j.enconman.2007.01.010.

[16] Pang S, Sharma MM. A model for predicting injectivity decline in water-injection wells. SPE Form Eval 1997;12(03):194–201. https://doi.org/10.2118/28489-pa.

[17] Peksa AE, Wolf K-H-A-A, Zitha PLJ. Bentheimer sandstone revisited for experimental purposes. Mar Pet Geol 2015;67:701–19. https://doi.org/10.1016/j.marpetgeo.2015.06.001.

[18] Por GJ, Boerrigter P, Maas JG, de Vries A. A fractured reservoir simulator capable of modeling block-block interaction. SPE Annual Tech Conf Exhib 1989.

[19] Raza A, Gholami R, Rezaee R, Bing CH, Nagarajan R, Hamid MA. CO_2 storage in depleted gas reservoirs: A study on the effect of residual gas saturation. Petroleum 2017;4:95–107.

[20] Regtien JMM, Por GJA, van Stiphout MT, van der Vlugt FF. Interactive Reservoir Simulation. SPE Reservoir Simulation Symposium 1995.

[21] Setzmann U, Wagner W. A new equation of state and tables of thermodynamic properties for methane covering the range from the melting line to 625 K at pressures up to 1000 MPa. J Phys Chem Ref Data 1991;20(6):1061–155.

[22] Soave G. Equilibrium constants from a modified Redlich-Kwong equation of state. Chem Eng Sci 1972;27(6):1197–203. https://doi.org/10.1016/0009-2509(72)80096-4.

[23] Span R, Wagner W. A new equation of state for carbon dioxide covering the fluid region from the triple-point temperature to 1100 K at pressures up to 800 MPa. J Phys Chem Ref Data 1996;25:1509–96.

[24] Springer, R., Anderko, A., & Miller, D. (2019). MSE-SRK: A Thermodynamic Model to Maximize the Accuracy of Predicting Phase Equilibria in Systems Containing Sour Gases, Electrolytes, and Hydrocarbons. Cedar Knolls, NJ: OLI Systems, Inc.

[25] Spycher N, Pruess K, Ennis-King J. CO_2-H_2O mixtures in the geological sequestration of CO_2. I. Assessment and calculation of mutual solubilities from 12 to 100°C and up to 600 bar. Geochim Cosmochim Acta 2003;67:3015–31. https://doi.org/10.1016/s0016-7037(03)00273-4.

[26] Wang P, Springer RD, Anderko A, Young RD. Modeling phase equilibria and speciation in mixed-solvent electrolyte systems. Fluid Phase Equilib 2004;222–223:11–7. https://doi.org/10.1016/j.fluid.2004.06.008.

[27] Xu J, Bu Z, Li H, Wang X, Liu S. Permeability models of hydrate-bearing sediments: a comprehensive review with focus on normalized permeability. Energies 2022;15(13):4524. https://www.mdpi.com/1996-1073/15/13/4524.